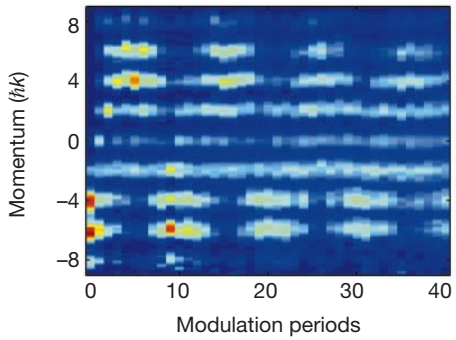

Figure 5 Momentum distributions as a function of the number of modulation periods, showing the tunnelling oscillation between negative and positive momenta. We note that the zero-momentum state remains mostly unpopulated, even when the mean momentum is zero. The colour coding ranges from blue to red for atomic populations ranging from small to large.

ity is that the tails of the oscillating quantum wave packets may extend outside the region of regular motion, allowing the atoms to 'leak out' into the classically chaotic region. This possibility is currently under investigation. The contribution of multiple Floquet states could lead to complicated multi-frequency oscillations, and an envelope for the tunnel oscillations appearing as decay, as observed for some parameters in our simulations. The effects of spontaneous emission and atom–atom interactions should be small.

Quantum theory predicts dynamical tunnelling to occur for various values of the scaled well depth κ, the modulation parameter ϵ and modulation frequency ω, and also predicts a strong sensitivity of the tunnelling period and amplitude on these parameters. For $\epsilon = 0.23$, $\kappa = 1.75$ and $\omega/2\pi = 250$ kHz we measured a tunnelling period of approximately 13 modulation periods. As shown in Fig. 4b, for $\epsilon = 0.30$, $\kappa = 1.82$ and $\omega/2\pi = 222$ kHz we find a tunnelling period of 6 modulation periods with a significantly longer decay time than in Fig. 4a. We have also experimentally observed an increase in the tunnelling period when κ is decreased and when all other parameters are held constant. This is the opposite of what one would expect for spatial barrier tunnelling.

Our observation of dynamical tunnelling of atoms in a modulated standing wave opens the door to further studies in quantum nonlinear dynamics. By varying the hamiltonian parameters and the initial conditions, we observe dynamical tunnelling for a variety of mixed phase space configurations. This may be 'chaos-assisted tunnelling', and a tunnelling rate that varies wildly as system parameters are changed would be a signature of such tunnelling[1]. By introducing noise or spontaneous emission in a controlled manner, we could systematically investigate the role of decoherence in tunnelling and explore the classical limit of chaotic systems. By carefully following the evolution of wave packets loaded into the chaotic region from a Bose–Einstein condensate, we could probe 'quantum chaos' with the unprecedented resolution afforded by minimum uncertainty wave packets.

During the preparation of this Letter, we learned of an experiment[14] reporting tunnelling of a different motional state in a similar system. □

Received 10 May; accepted 12 June 2001.

1. Tomsovic, S. Tunneling and chaos. *Physica Scripta T* **90,** 162–165 (2001).
2. Caldeira, A. O. & Leggett, A. J. Quantum tunneling in a dissipative system. *Ann. Phys.* **149,** 374–456 (1983).
3. Davis, M. J. & Heller, E. J. Quantum dynamical tunneling in bound states. *J. Chem Phys.* **75,** 246–254 (1981).
4. Dyrting, S., Milburn, G. J. & Holmes, C. A. Nonlinear quantum dynamics at a classical second order resonance. *Phys. Rev. E* **48,** 969–978 (1993).
5. Haake, F., Kus, M. & Scharf, R. Classical and quantum chaos for a kicked top. *Z. Phys. B* **65,** 381–395 (1987).
6. Sanders, B. C. & Milburn, G. J. The effect of measurement on the quantum features of a chaotic system. *Z. Phys. B* **77,** 497–510 (1989).
7. Habib, S., Shizume, K. & Zurek, W. H. Decoherence, chaos, and the correspondence principle. *Phys. Rev. Lett.* **80,** 4361–4365 (1998).
8. Graham, R., Schlautmann, M. & Zoller, P. Dynamical localization of atomic-beam deflection by a modulated standing light wave. *Phys. Rev. A* **45,** R19–R22 (1992).
9. Moore, F. L., Robinson, J. C., Bharucha, C. F., Sundaram, B. & Raizen, M. G. Atom optics realization of the quantum δ-kicked rotor. *Phys. Rev. Lett.* **75,** 4598–4601 (1995).
10. Hensinger, W. K., Truscott, A. G., Upcroft, B., Heckenberg, N. R. & Rubinsztein-Dunlop, H. Atoms in an amplitude-modulated standing wave–dynamics and pathways to quantum chaos. *J. Opt. B* **2,** 659–667 (2000).
11. Hensinger, W. K. *et al.* Experimental study of the quantum driven pendulum and its classical analog in atom optics. *Phys. Rev. A* (in the press).
12. Arnold, V. I. *Mathematical Methods of Classical Mechanics* (Springer, New York, 1979).
13. Kozuma, M. *et al.* Coherent splitting of Bose-Einstein condensed atoms with optically induced Bragg diffraction. *Phys. Rev. Lett.* **82,** 871–875 (1999).
14. Steck, D. A., Oskay, W. H. & Raizen, M. G. Observation of chaos-assisted tunneling between islands of stability. *Science* (in the press).

Acknowledgements

We thank C. Holmes for discussions. The NIST group was supported by the ONR, NASA and ARDA, and the University of Queensland group was supported by the ARC. A.B. was partially supported by DGA (France), and H. H. was partially supported by the A. v. Humboldt Foundation. W.K.H. and B.U. thank NIST for hospitality during the experiments.

Correspondence and requests for materials should be addressed to W.K.H. (e-mail: hensinge@physics.uq.edu.au).

Quantum interference of superfluid ^{3}He

R. W. Simmonds, A. Marchenkov, E. Hoskinson, J. C. Davis & R. E. Packard

Physics Department, University of California, Berkeley, California 94720, USA

Celebrated interference experiments have demonstrated the wave nature of light[1] and electrons[2], quantum interference being the manifestation of wave–particle duality. More recently, double-path interference experiments have also demonstrated the quantum-wave nature of beams of neutrons[3], atoms[4] and Bose–Einstein condensates[5]. In condensed matter systems, double-path quantum interference is observed in the d.c. superconducting quantum interference device[6] (d.c. SQUID). Here we report a double-path quantum interference experiment involving a liquid: superfluid ^{3}He. Using a geometry analogous to the superconducting d.c. SQUID, we control a quantum phase shift by using the rotation of the Earth, and find the classic interference pattern with periodicity determined by the ^{3}He quantum of circulation.

Our basic interferometer topology is shown in Fig. 1a. Schematically, the device is a circular loop of radius R which includes two superfluid ^{3}He Josephson weak links[7,8]. These weak links each consist of a 65 × 65 array of 100-nm apertures etched in a 60-nm-thick silicon nitride membrane. Similar arrays have previously been shown to be characterized by a current–phase relation given[9] by the Josephson formula:

$$I = I_c \sin\phi \qquad (1)$$

Here I is the mass current flowing through the array, ϕ is the quantum phase difference across the array, and I_c is the critical current characterizing the array.

The interferometer is predicted to behave as a single weak link with an effective critical current, I_c^* (see Methods). If the inter-

ferometer is rotated at angular velocity $\mathbf{\Omega}$, I_c^* is modulated by an interference term[10]

$$I_c^* = 2I_c\left|\cos\left(\pi\frac{2\mathbf{\Omega}\cdot\mathbf{A}}{\kappa_3}\right)\right| \quad (2)$$

where $\mathbf{A}$ is the area vector of the loop and $\kappa_3 \equiv h/(2m_3)$ is the ^{3}He quantum of circulation. Thus the effective critical current is predicted to be modulated with a period determined by the rotation flux through the interferometer, analogous to the manner in which magnetic flux modulates the critical current of a d.c. SQUID.

The interference occurs because the phase of the superfluid wavefunction receives equal and opposite shifts in the two arms of the interferometer. The phase shift arising from the rotation flux is identical in form to that in other neutral-matter quantum rotation interferometers[3,11], as well as in the optical Sagnac interferometer[12] if the photon effective mass is taken to be $\hbar\omega/c^2$.

The goal of our experiment is to demonstrate two ideas. (1) That the superfluid interferometer is indeed characterized as a single weak link with a well defined critical current I_c^*, and (2) that by changing the orientation of the plane of the loop with respect to the Earth's rotation vector, the current I_c^* can be modulated according to the interference term in equation (2). I_c^* should exhibit periodicity of $(2\mathbf{\Omega}\cdot\mathbf{A})/\kappa_3$.

A geometrically more accurate sketch of our interferometer is shown in Fig. 1b. The quantum phase difference across the interferometer should evolve according to the equation[13]:

$$\Phi = -\int\frac{2m_3}{\rho\hbar}P(t)\mathrm{d}t \quad (3)$$

where ρ is the density of the liquid and P is the pressure differential across the ends of the device. So if the interferometer behaves as a single Josephson weak link, a static pressure P_0 applied across the interferometer will cause the quantum phase to increase linearly in time, leading to mass current oscillations at a Josephson frequency[8]:

$$\omega_j = \frac{2m_3}{\hbar\rho}P_0 \quad (4)$$

As described in Fig. 1 legend, the deflection of the flexible membrane reveals both the pressure across the interferometer and the mass current through it. We have developed a feedback method that permits us to drive the system at constant pressure by applying a time-varying voltage to the membrane. We select a pressure for which the Josephson frequency lies near 270 Hz, a spectral region away from parasitic acoustic noise lines in the displacement transducer.

Figure 2 shows a Fourier transform of the mass current through the interferometer that results from the constant-pressure drive being applied for about 6 seconds. A sharp peak at 273 Hz is clearly visible. This corresponds to the Josephson oscillation. This

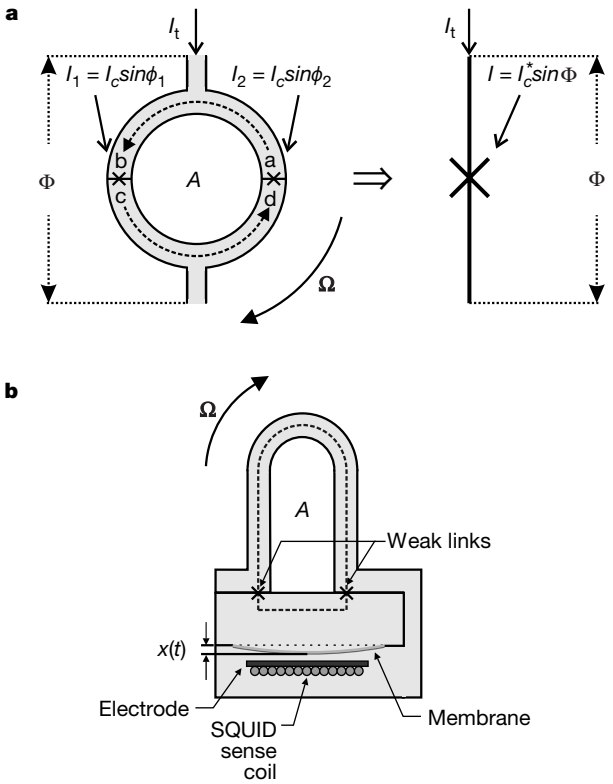

Figure 1 Two views of our superfluid quantum interferometer. **a**, Schematic diagram of the basic interferometer loop. As shown in the Methods section, the total current through the two sides of the loop (I_t) is predicted to depend on the total phase difference across the loop, Φ, as given by equation (1) with I_c replaced by I_c^* (given by equation (2)). **b**, The interferometer geometry used in this experiment. Although the two weak links are moved closer together, the topology is unchanged and I_c^* is still given by equation (2). The nominal 'loop' area, A, is ~6 cm^2, and the tube cross-sectional diameter is ~0.3 cm. Pressure differences can be applied to the flexible metallized membrane (and hence across the two weak links) by applying voltages between it and the adjacent rigid electrode. The membrane is coated with a superconducting film. The sense coil contains a trapped persistent current which is partially shunted into the input coil of a d.c. SQUID if the membrane moves[26]. Knowledge of the deflection of the membrane, $x(t)$, reveals the pressure head across the interferometer. The rate of change of the deflection reveals the mass current through the interferometer. The noise in the displacement sensor is 2×10^{-15} m Hz$^{-1/2}$. We use a feedback system that applies a voltage to the electrode such that the pressure across the interferometer is fixed at some predetermined value, typically near 1.5 mPa. Temperature is monitored with two thermometers, one using platinum nuclear magnetic resonance and a second using lanthanum cerium magnesium nitrate (LCMN). The experiment is performed at zero ambient pressure.

frequency agrees with equation (4) to within the systematic uncertainty (~10%) in the electrostatically derived calibration of the pressure scale. We have determined that the oscillation frequency scales linearly with P_0 at least up to 1 kHz, and that there is no higher-harmonic signal detectable with the present signal-to-noise ratio. This implies that the overall current–phase relation is sine-like, and that the two separated arrays are phase coherent. The area under the Josephson oscillation peak in Fig. 2 is proportional to I_c^*, the critical current for the interferometer.

This oscillation signal results from the quantum coherence among all the apertures in each array, as well as between both arrays. Thus, not only are both weak links themselves coherent, but the $\sim 10^{22}$ atoms within the torus are also quantum phase coherent with them. This demonstrates the first point, that the interferometer behaves as a single Josephson weak link with a well defined critical current, I_c^*.

Furthermore, weak-link arrays have previously been shown[14] to exhibit a characteristic rigid-pendulum oscillation mode whose small-amplitude frequency ω_p is proportional to $\sqrt{I_c}$. We have observed this normal mode motion in our interferometer and find $\omega_p \propto \sqrt{I_c^*}$, again confirming that the device behaves as a single weak link characterized by equations (1) and (3).

The second goal of our experiment is to see if phase gradients, generated by absolute rotation of the loop, create an interference pattern to modulate I_c^*, as predicted in equation (2). We chose the loop area A to be 6 cm^2 so that the rotation of the Earth, $\mathbf{\Omega}_E$, can itself lead to several periods of the modulation pattern. The plane of the loop is vertical—that is, the vector $\mathbf{A}$ points horizontally in the laboratory. Thus we can vary the rotation flux in the loop, $\mathbf{\Omega}_E \cdot \mathbf{A}$, by reorienting the interferometer about a vertical axis in the laboratory frame. This reorientation technique was used previously in superfluid ^{4}He to show that rotation flux could vary the phase-slip critical velocity in an aperture[15,16]. Other experiments employed reorientation of a superfluid ^{3}He loop to change the frequency in a nonlinear Helmholtz oscillator[17,18] containing a single Josephson weak link.

Figure 3 shows the result of our reorientation experiment. We plot the normalized measured current magnitude I_c^* as a function of $(2\mathbf{\Omega}\cdot\mathbf{A})/\kappa_3$. The data reveal the double-path quantum interference pattern. The solid curve is the interference pattern expected from equation (2). The periodicity of the observed interference pattern is found to be as predicted: $(2\mathbf{\Omega}\cdot\mathbf{A})/\kappa_3$, within the experimental precision (which is limited by knowledge of the loop area).

The interference pattern predicted by equation (2) and shown in Fig. 3 is the central feature of this experiment. The device displays a remarkable phenomenon: two-path quantum interference in a liquid. The pattern shows that the interferometer is indeed the superfluid equivalent of a d.c. SQUID.

It is natural to ask if the superfluid quantum interference device could be developed into a sensitive rotation sensor[19–21], perhaps to perform meaningful geodesy measurements or experiments on general relativity. Following the analysis[22] of superconducting d.c. SQUIDs, the intrinsic noise in this type of device arises from Nyquist noise in the various dissipative processes associated with the weak links themselves[23]. The potential intrinsic sensitivity can only be reached if other extrinsic noise sources—such as temperature drifts, environmental noise and electronic SQUID readout noise—are reduced by orders of magnitude from the values in the present experiment.

We have demonstrated a double-path superfluid interferometer which is the analogue of a d.c. SQUID. The entire interferometer exhibits dynamic behaviour (Josephson oscillations and pendulum motion) similar to that of a single weak link. Owing to quantum interference, the effective critical current is modulated by rotation flux through the enclosed area. Our double-path interference

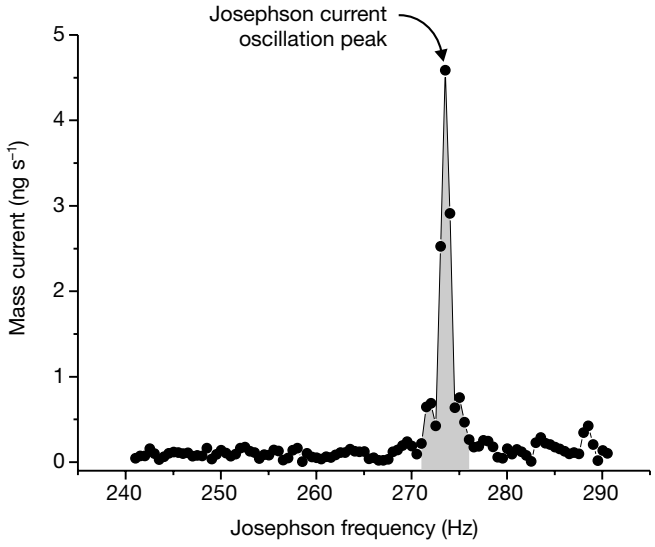

Figure 2 The spectrum of the mass current during a 2-s interval of the data stream from the SQUID position transducer. A typical data stream is 6 s long, limited by the magnitude of the voltage we can apply to the diaphragm. Due to imperfect pressure regulation, the Josephson peak drifts slightly during the 6-s data stream. So we break the transient into 2-s intervals, and use a fast Fourier transform (FFT) routine to produce a figure like that above for each interval. The peak is due to Josephson oscillations at 273 Hz. We compute a number proportional to the area under the peak (shaded in the figure). At a fixed orientation we record multiple data streams (typically 17), and average the resultant areas. This average is taken as the measure of I_c^*, the critical current of the interferometer.

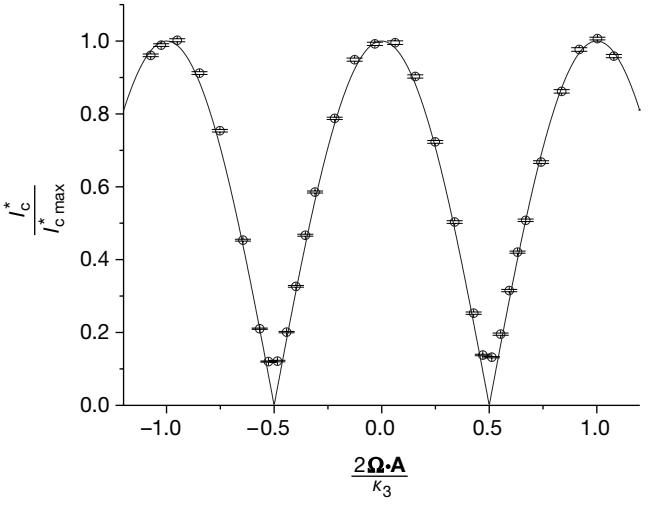

Figure 3 The interference pattern of a superfluid quantum interference gyroscope. The figure shows a plot of the effective critical current I_c^* as a function of $(2\mathbf{\Omega}\cdot\mathbf{A})/\kappa_3$, where κ_3 is the quantum of circulation (see equation (2)). The error bars, which are the standard error of typically 100 FFTs, are smaller than the size of the plotted points. The temperature was approximately $0.8T_c$, where T_c is the critical temperature of the superfluid. We have applied a temperature correction (no greater than 4%) to account for systematic errors from small temperature drifts recorded by the LCMN during the course of the measurement. The rotation flux was varied by reorienting the normal to the loop's plane through an angle of $\pm\pi/2$ with respect to the east–west direction. Then the rotation flux $\mathbf{\Omega}\cdot\mathbf{A}$ is equal to $\Omega_E A \cos\theta_L \sin\Theta$, where Θ is the direction of $\mathbf{A}$ with respect to an east–west line, and $\theta_L \approx 38°$ is the latitude of Berkeley. The solid line is a plot of equation (2).

experiment advances the close analogy between the macroscopic quantum physics of superconductivity and superfluidity. Both systems exhibit persistent currents, quantized circulation (fluid and magnetic), sinϕ weak links and now, double-path quantum interference. □

Methods

To derive equation (2) we follow a heuristic method similar to that which Feynman[24] applied to the analogous superconducting case. Consider the interferometer in Fig. 1a to be rotating at angular velocity Ω. The total external current passing through the interferometer may be written as:

$$I_t = I_c \sin\phi_1 + I_c \sin\phi_2 = 2I_c \cos\left(\frac{\phi_1 - \phi_2}{2}\right)\sin\left(\frac{\phi_1 + \phi_2}{2}\right) \quad (5)$$

We assume that the fluid in the torus is characterized at every point by a quantum phase factor which is macroscopically coherent. The rotation of the torus entrains the superflow which is then almost that of a solid body, $v_s = \Omega R$. Around a closed path in the interferometer, as indicated by the dotted line in Fig. 1, the phase can change only in multiples of 2π.

$$\oint \nabla\phi \cdot d\mathbf{l} = 2\pi n = \int_a^b \frac{2m_3}{\hbar} \mathbf{v}_s \cdot d\mathbf{l} + \phi_1 + \int_c^d \frac{2m_3}{\hbar} \mathbf{v}_s \cdot d\mathbf{l} - \phi_2 = -\frac{2m_3}{\hbar} 2\Omega\pi R^2 + \phi_1 - \phi_2 \quad (6)$$

The limit points, a–d, in the integrals are shown in Fig. 1a. In equation (6) we have used the concept[25] that the phase gradient is proportional to superfluid velocity, $\nabla\phi = (2m_3\mathbf{v}_s)/\hbar$. Equation (6) may be solved for $\phi_1 - \phi_2$, which, when inserted into equation (5) gives

$$I_t = I_c^* \sin\Phi \quad (7)$$

where $\Phi \equiv (\phi_1 + \phi_2)/2$ is the phase difference across the ends of the interferometer. We see that the rotating interferometer behaves as a single Josephson weak link, whose maximum current is given by the quantum interference term:

$$I_c^* = 2I_c \left|\cos\left(\pi \frac{2\Omega \cdot \mathbf{A}}{\kappa_3}\right)\right| \quad (8)$$

Here $\kappa_3 \equiv \hbar/(2m_3)$ is the quantum of circulation, **A** is the interferometer area vector, normal to the plane, and we have included a scalar product describing the more general case when the rotation axis is not parallel to **A**.

Received 5 March; accepted 14 May 2001.

1. Young, T. *A Course of Lectures in Natural Philosophy and the Mechanical Arts* Vol. 1, 364 (London, 1845); also as facsimile edition (New York, 1971).
2. Davisson, C. J. Are Electrons Waves? *Franklin Inst. J.* **205,** 597 (1928).
3. Werner, S. A., Studenmann, J. L. & Colella, R. Effect of Earth's rotation on the quantum mechanical phase of the neutron. *Phys. Rev. Lett.* **42,** 1103–1106 (1979).
4. Keith, D. W., Ekstrom, C. R., Turchette, Q. A. & Pritchard, D. E. An interferometer for atoms. *Phys. Rev. Lett.* **66,** 2693–2696 (1991).
5. Andrews, M. R. *et al.* Observation of interference between two Bose condensates. *Science* **275,** 637–641 (1997).
6. Barone, A. & Paterno, G. *Physics and Application of the Josephson Effect* (Wiley, New York, 1982).
7. Varoquaux, E. & Avenel, O. Josephson effect and quantum phase slippage in superfluids. *Phys. Rev. Lett.* **60,** 416–419 (1988).
8. Pereversev, S. V., Loshak, A., Backhaus, S., Davis, J. C. & Packard, R. E. Quantum oscillations between two weakly coupled reservoirs of superfluid ^{3}He. *Nature* **388,** 449–451 (1997).
9. Marchenkov, A. *et al.* Bi-state superfluid ^{3}He weak links and the stability of Josephson π states. *Phys. Rev. Lett.* **83,** 3860–3863 (1999).
10. Packard, R. E. & Vitale, S. Principle of superfluid-helium gyroscopes. *Phys. Rev. B* **46,** 3540–3549 (1992).
11. Gustavson, T. L., Bouyer, P. & Kasevitch, M. A. Physical rotation measurements with an atom interferometer gyroscope. *Phys. Rev. Lett.* **78,** 2046–2049 (1997).
12. Stedman, G. E. Ring-laser tests of fundamental physics and geophysics. *Rep. Prog. Phys.* **60,** 615–687 (1997).
13. Anderson, P. W. in *Progress in Low Temperature Physics* (ed. Gorter, C. J.) 1–44 (North Holland, Amsterdam, 1967).
14. Marchenkov, A., Simmonds, R. W., Davis, J. C. & Packard, R. E. Observation of the Josephson plasma mode for a superfluid ^{3}He weak link. *Phys. Rev. B* **61,** 4196–4199 (2000).
15. Schwab, K., Bruckner, N. & Packard, R. E. Detection of the Earth's rotations using superfluid phase coherence. *Nature* **386,** 585–587 (1997).
16. Avenel, O., Hakonen, P. & Varoquaux, E. Detection of the rotation of the Earth with a superfluid gyrometer. *Phys. Rev. Lett.* **78,** 3602–3605 (1997).
17. Mukharsky, Yu., Varoquaux, E. & Avenel, O. Current-phase relationship measurements in the flow of superfluid ^{3}He through a single orifice. *Physica B* **280,** 130–131 (2000).
18. Mukharsky, Yu., Avenel, O. & Varoquaux, E. Rotation measurements with a superfluid ^{3}He gyrometer. *Physica B* **284–288,** 287–288 (2000).
19. Rowe, C. H. *et al.* Design and operation of a very large ring laser gyroscope. *Appl. Opt.* **38,** 2516–2523 (1999).
20. Gustavson, T. L., Landragin, A. & Kasevich, M. A. Rotation sensing with a dual atom interferometer Sagnac gyroscope. *Class. Quant. Gravity* **17,** 2385–2398 (2000).
21. Herring, T. A. The rotation of the Earth. *Rev. Geophys. Suppl.* **29,** 172–175 (1991).
22. Clarke, J. in *SQUID Sensors: Fundamentals, Fabrication and Applications* (ed. Weinstock, H.) (Kluwer Academic, 1996).
23. Simmonds, R. W., Marchnkov, A., Vitale, S., Davis, J. C. & Packard, R. E. New flow dissipation mechanisms in superfluid ^{3}He. *Phys. Rev. Lett.* **84,** 6062–6065 (2000).
24. Feynmann, R. P., Leighton, R. B. & Sands, M. *The Feynman Lectures in Physics* Vol. 3, Ch. 21 (Addison Wesley, Reading, Massachusetts, 1963).
25. Tilley, D. R. & Tilley, J. *Superfluidity and Superconductivity* 3rd edn 171 (Hilger, Bristol, 1990).
26. Paik, H. J. Superconducting tunable-diaphragm transducer for sensitive acceleration measurements. *J. Appl. Phys.* **47,** 1168–1178 (1976).

Acknowledgements

We thank S. Vitale and K. Penanen for discussions; Y. Sato for assistance; A. Loshak for making the aperture arrays; and E. Crump, D. Mathews and C. Ku for assistance in improving noise conditions in our building. This work was supported in part by NASA, the Office of Naval Research, the National Science Foundation, and the Miller Institute for Basic Research (J.C.D.).

Correspondence and requests for materials should be addressed to R.P. (e-mail: packard@socrates.berkeley.edu).

Coexistence of superconductivity and ferromagnetism in the *d*-band metal $ZrZn_2$

C. Pfleiderer*, M. Uhlarz*, S. M. Hayden†, R. Vollmer*, H. v. Löhneysen*‡, N. R. Bernhoeft§ & G. G. Lonzarich‖

* *Physikalisches Institut, Universität Karlsruhe, D-76128 Karlsruhe, Germany*
† *H. H. Wills Physics Laboratory, University of Bristol, Bristol BS8 1TL, UK*
‡ *Forschungszentrum Karlsruhe, Institut für Festkörperphysik, D-76021 Karlsruhe, Germany*
§ *DRFMC-SPSMS, CEA Grenoble, F-38054 Grenoble, Cedex 9, France*
‖ *Cavendish Laboratory, University of Cambridge, Madingley Road, Cambridge CB3 0HE, UK*

It has generally been believed that, within the context of the Bardeen–Cooper–Schrieffer (BCS) theory of superconductivity, the conduction electrons in a metal cannot be both ferromagnetically ordered and superconducting[1,2]. Even when the superconductivity has been interpreted as arising from magnetic mediation of the paired electrons, it was thought that the superconducting state occurs in the paramagnetic phase[3,4]. Here we report the observation of superconductivity in the ferromagnetically ordered phase of the *d*-electron compound $ZrZn_2$. The specific heat anomaly associated with the superconducting transition in this material appears to be absent, and the superconducting state is very sensitive to defects, occurring only in very pure samples. Under hydrostatic pressure superconductivity and ferromagnetism disappear at the same pressure, so the ferromagnetic state appears to be a prerequisite for superconductivity. When combined with the recent observation of superconductivity in UGe_2 (ref. 4), our results suggest that metallic ferromagnets may universally become superconducting when the magnetization is small.

The compound $ZrZn_2$ was first investigated by Matthias and Bozorth[5] in the 1950s, who discovered that it was ferromagnetic despite being made from nonmagnetic, superconducting constituents. $ZrZn_2$ crystallizes in the C15 cubic Laves structure, as shown in the inset of Fig. 1, with lattice constant $a = 7.393$ Å. The Zr atoms form a tetrahedrally coordinated diamond structure and the magnetic properties of the compound derive from the Zr 4*d* orbitals, which have a significant direct overlap[6]. Ferromagnetism develops